MTLA 28 (2023) 101764

Contents lists available at ScienceDirect

Materialia

journal homepage: www.elsevier.com/locate/mtla

Assessing the high concentration of vacancies in refractory high entropy alloys

Jack A. Wilson [a,*], Christopher Moore [a], David T. Goddard [b], Simon C. Middleburgh [a]

[a] Nuclear Futures Institute, Bangor University, Bangor LL57 1UT, United Kingdom
[b] National Nuclear Laboratory, Preston Laboratory, Springfields, Preston, Lancashire PR4 0XJ, United Kingdom

ARTICLE INFO

Keywords:
Vacancy formation energy
High entropy alloy
Defect formation
Atomistic modelling

ABSTRACT

Accurate determination of monovacancy formation enthalpy is vital for work on diffusion, melting point determination of high temperature materials, radiation damage, and thermophysical stability of alloys. These enthalpies take on a single value in pure metals but is made more complex in concentrated solid solutions due to the local chemical environments possible around each vacancy. Herein, using first-principles density functional theory, we report the distributions of vacancy formation enthalpies in 21 equiatomic 5-component solid-solution alloys from the Hf-Mo-Nb-Ta-Ti-W-Zr system. Chemical disorder is treated using the special quasi-random structure method, and the chemical potential of vacant element is treated by approximating it to its total energy in its standard state. We find that the highest vacancy formation enthalpies belong to the MoNbTaTiW alloy (which incidentally is the most reported in literature) and the lowest belongs to HfNbTaTiZr, with other alloys in-between. We use the whole distribution of formation enthalpies to estimate the equilibrium concentration of vacancies as a function of temperature.

1. Introduction

High entropy alloys (HEAs), sometimes referred to as compositionally complex alloys, multicomponent element alloys, or concentrated solid solutions, pioneered by Cantor et al. [1] and Yeh et al. [2], offer innovative multi-component alloy compositions for extreme environment materials such as in the nuclear [3,4] or aerospace [5] industries. Originally defined as having 5 or more elements in high concentrations (5 – 35 at%) [2], high entropy alloys could offer superior properties, including strength and hardness [6,7], oxidation resistance [8–11], and high thermal stability [12]. Vacancies, their formation energies, and their equilibrium concentration have been studied for their role in diffusion kinetics [13], precipitation [14], radiation resistance [13,15,16], and material properties such as strength [17,18]. HEAs are observed to have higher concentrations of vacancy defects compared to conventional alloys [18,19]. The exact mechanism behind this higher concentration is not yet fully understood.

Wang et al. presented a thermodynamic analysis which concludes that configurational entropy causes a substantial increase in equilibrium vacancy concentrations in high entropy alloys compared to pure metals and binary alloys [19]. Contrary to this, Daigle et al. propose that configurational entropy reduces the equilibrium vacancy concentration in high entropy materials [20]. This viewpoint is supported by Jodi et al., who demonstrated that alloys with higher configurational entropy in the $Fe_x(CoCrMnNi)_{100-x}$ system had lower equilibrium concentrations of monovacancies, although the authors attributed this to the compositional effect of Fe on the vacancy formation enthalpy [21]. Daigle et al. suggests that most equilibrium vacancies in high entropy materials are produced from the lower tails of the vacancy formation enthalpy distribution, which tend to be significantly lower than the mean. This results in an enhanced vacancy concentration in complex materials such as HEAs, compared to conventional alloys and pure metals [20].

Experimental research on vacancy formation in HEAs predominantly relies on positron annihilation lifetime spectroscopy [21,22] and tracer diffusion experiments [23], but presently, few of these studies have been performed. To support experimental efforts, recent advances in density functional theory [24,25], molecular dynamics [26], and machine learning models [27] have enabled the study of vacancy formation in compositionally complex alloys such as HEAs. Many previous studies on vacancy formation enthalpies of compositionally complex alloys have focussed on the Cantor alloy [28] and derivative alloys thereof [22,25,29–34], although studies on some refractory alloys do exist [24,35–38].

* Corresponding author.
E-mail address: jack.wilson@bangor.ac.uk (J.A. Wilson).

https://doi.org/10.1016/j.mtla.2023.101764
Received 29 March 2023; Accepted 1 April 2023
Available online 2 April 2023

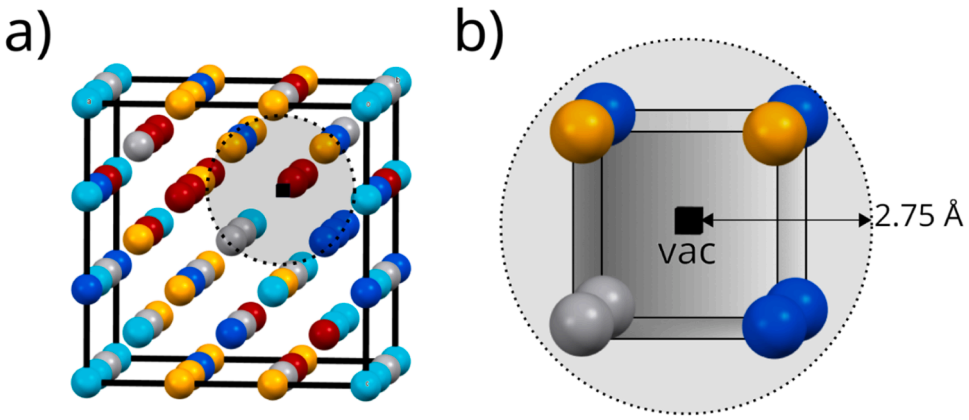

Fig. 1. Vacancy volume of body-centred cubic supercells. a) vacancy within a body-centred cubic supercell, and b) atoms within the cut off radius used to calculate vacancy volume.

For example, Cunliffe et al. proposed a method to calculate the vacancy formation enthalpy in multi-component amorphous alloys, including refractory alloys, which involves averaging the vacancy formation enthalpy of the respective pure metals [37]. Roy et al. determined the vacancy formation energy of $(Mo_{0.95}W_{0.05})_{0.85}Ta_{0.10}(TiZr)_{0.05}$ via density functional theory to be between 2.87 – 3.84 eV [35]. Zhang et al. investigated vacancy energetics in the Al-Hf-*Sc*-Ti-Zr system, including the binary to quaternary alloys. From this, they calculated the temperature dependence of the Gibbs energy of vacancy formation [24]. Zhao et al. determined the vacancy formation enthalpy of CrTaVW to be between 2.45 – 3.94 eV, with a mean value of 3.18 eV [39]. The literature however remains sparse on thorough interrogations of vacancy formation enthalpies in refractory HEAs.

Using density functional theory, we examine the vacancy formation enthalpies of all quinary alloys in the seven-element Hf-Mo-Nb-Ta-Ti-W-Zr system. The formation enthalpies of vacancies and their trends are presented. We show that refractory solid solutions have higher equilibrium vacancy concentrations than pure elements. Rather than the configurational entropy being the cause of this, vacancy formation energies at the lower-end tail of the vacancy formation energy distribution are responsible for the higher equilibrium vacancy concentrations observed in high entropy alloys. These findings suggest important phenomena that may dictate in the migration of defects (intrinsic and extrinsic) that will influence phenomena including: phase segregation, corrosion, radiation damage accumulation/recovery and mechanical properties.

2. Methodology

2.1. Special quasi-random structure supercells

Density functional theory [40,41] is computationally intensive (generally limited to hundreds of atoms at a time). The conventional way to capture bulk material properties is to use periodic boundary conditions, but this imposes non-random periodicity on simulations, which poses challenges for modelling infinitely random lattices in density functional theory computations. Special quasi-random structures (SQS) attempt to replicate random materials by matching correlation functions between pairs of atoms within a defined cut-off radius (short-range interactions are more dominant than long-range interactions) to capture bulk random lattice features. In this study, special quasi-random structures were constructed using the mcsqs code in the Alloy Theoretic Automated Toolkit [42] similar to previous work [38]. We set cut-off distances to include up to third nearest neighbour pair interactions. We did not consider triplet and higher order interactions.

2.2. Total energy relaxations

Density function theory [40,41] structural relaxation calculations at constant pressure were based on the plane wave pseudopotential approach as implemented in the Vienna *ab initio* simulation package VASP [43,44] version 5.4.4. Projector augmented-wave (PAW) pseudopotentials are used [45,46]. Electrons treated as valence are: Hf: 10, Mo: 14, Nb: 13, Ta: 11, Ti: 12, W: 12, and Zr: 12. The Perdew, Burke, and Ernzerhof version of the generalised gradient approximation exchange-correlation functional was applied [47]. Cut-off energy for plane waves were set to 500 eV for all calculations. A Methfessel-Paxton smearing width of 2 eV was used [48]. A K-point mesh was selected based on convergence of the total energy to 0.01 eV/atom which resulted in a $4 \times 4 \times 4$ Γ-centred mesh for all cells. Convergence testing for plane wave cut off energies and K-points can be found in **Supplementary Figures S1–2**.

2.3. Calculating local bias

We adopt a measure for how the immediate environment of a vacancy is biased towards particular elements using nomenclature from Li et al. [33]. For example, for a vacancy in a body-centred cubic lattice surrounded by 8 atoms of elements A, B, C, D and E, a measure of (2,2,2,1,1), respectively would indicate a relatively unbiased vacancy without predilection for any particular element. A measure of (5,3,0,0,0) indicates a biased local arrangement, and a measure of (8,0,0,0,0) indicates that all local atoms within an appropriate cut off distance are of a single element, A. From this notation, we calculate an overall measure of local element bias per vacancy via

$$local\ element\ bias = \sqrt{\frac{1}{N}\sum_{i=element\ A}^{E}(j_i - nx_i)^2} \quad (1)$$

Where N is the total number of elements in the alloy, n is the coordination number (8 for body-centred cubic, 12 for face-centred cubic and hexagonal close-packed), x_j is the atomic fraction of element j, j is the number atoms of each element, A to E, surrounding a vacancy, and $\bar{j}$ is the mean number of atoms of each elements surrounding vacancies in an infinitely random solid solution (calculated to be 1.6 for an equiatomic quinary body-centred cubic alloy). and Eq. (1) resembles that of the root-mean-square deviation. For the previous examples, (2,2,2,1,1), (5,3,0,0,0), and (8,0,0,0,0), we respectively obtain local element biases of 1.04, 3.46, and 4.29, with more examples listed in **Supplementary Table S1**. Each alloy is assumed to be completely equiatomic amongst constituent elements in Eq. (1) and has negligible effect on the biases calculated (**Supplementary Figure S3**).

2.4. Calculating vacancy volumes

Vacancy volume is calculated by calculating the volume of the convex hull constructed between coordinates of the nearest neighbour atoms to the vacancy chosen with a cut off distance of 2.75 Å to include first nearest neighbours but exclude second and further nearest neighbours. Fig. 1a illustrates a body-centred cubic 53-atom cell with a vacancy. Fig. 1b indicates the cut off radius around the vacancy used to calculate the vacancy volume. However, in some alloys with large lattice strain some 9 or so neighbours can exist within the cut off distance. Due to the small number of these occurrences, we therefore treat all these atoms as 1st nearest neighbours similar to previous work [27] for calculations involving local bias or vacancy volume.

2.5. Vacancy formation energy calculations

Vacancy formation enthalpies were calculated by structurally relaxing each 54-atom supercell at constant pressure. Each atom was then removed in turn, and the supercell allowed to relax around the vacancy, again, at constant pressure. The vacancy formation enthalpy, H_f^v, is calculated via

$$H_f^v = E_v - E_0 + \mu_v \tag{2}$$

where E_v is the total energy of the supercell containing a vacancy, E_0 is the total energy of the supercell without a vacancy, and μ_v is the chemical potential of the removed species. The sign of μ_v corresponds to either a vacancy (+ sign) or an interstitial (- sign). In the literature, variation of μ_v in bulk metals versus in complex alloys were found to be insignificant [25,35,39]. For example, Roy et al. investigated the relationship between μ_v in the refractory Mo-Ta-Ti-W-Zr system and their constituent pure metals and found that the chemical potential differed by less than 1.1% [35]. Herein, we approximate the chemical potential of the defect species as that in its bulk metal form via the equation

$$H_f^v = E_v - E_0 + E_{defect} \tag{3}$$

where E_{defect} is the total energy, normalised to energy-per-atom, of the pure metal in its bulk form at 0 K (hexagonal close packed Hf, Ti, and Zr, and body-centred cubic Mo, Nb, Ta, and W). The accuracy of these pure bulk metal lattice energy calculations was similar to that of the alloy supercells.

2.6. General calculation information

Each supercell afforded 54 unique vacancy formation enthalpies. These were calculated at least in duplicate for each quinary alloy in the Hf-Mo-Nb-Ta-Ti-W-Zr system (using a different special quasi-random structure supercell each time), yielding a total of at least 108 vacancy formation enthalpies per alloy. The element whose number of atoms is slightly deficient in each supercell, was allowed to vary at random, and no significant effect of this was observed in the resulting distributions of vacancy formation enthalpies (via a two-tailed Kolmogorov-Smirnov test). Datasets and calculation outputs will be made available on request to the author.

To interrogate any correlations between vacancy formation enthalpy and bulk properties, such that H_f^v might be predicted using easily obtained properties, the Pearson product-moment correlation coefficient between H_f^v and several properties were calculated including electron valence concentration, atomic size mismatch factor, and lattice parameter. These properties are easily obtained via the parametric approach to phase stability of concentrated solid solution alloys [49–51].

Table 1
Thermophysical parameters for equiatomic alloys. ΔH_{mix}, δ, VEC, γ, and Ω.

composition	ΔH_{mix} (kJmol^{-1})	δ (%)	VEC	γ	Ω
HfMoNbTaTi	−1.44	6.23	4.8	1.0526	24.87
HfMoNbTaW	−4.64	3.51	5.2	1.0717	8.73
HfMoNbTaZr	−1.12	3.56	4.8	1.0341	32.42
HfMoNbTiW	−4.48	6.06	5	1.0719	8.24
HfMoNbTiZr	−1.6	6.68	4.6	1.0523	20.44
HfMoNbWZr	−4.96	3.94	5	1.0712	7.54
HfMoTaTiW	−4.48	6.18	5	1.0719	8.56
HfMoTaTiZr	−1.92	6.73	4.6	1.0523	17.79
HfMoTaWZr	−4.96	3.94	5	1.0712	7.83
HfMoTiWZr	−5.6	6.7	4.8	1.0714	6.29
HfNbTaTiW	−2.72	6.11	4.8	1.0719	13.95
HfNbTaTiZr	2.72	6.46	4.4	1.0523	12.41
HfNbTaWZr	−2.56	3.03	4.8	1.0712	15.02
HfNbTiWZr	−3.04	3.03	4.8	1.0714	11.46
HfTaTiWZr	−3.36	3.03	4.8	1.0714	10.8
MoNbTaTiW	−5.28	4.95	5.2	1.0362	7.39
MoNbTaTiZr	−1.76	5.97	4.8	1.0526	19.77
MoNbTaWZr	−5.44	3.16	5.2	1.0717	7.26
MoNbTiWZr	−5.28	5.75	5	1.0719	6.8
MoTaTiWZr	−5.28	5.88	5	1.0719	7.07
NbTaTiWZr	−3.2	5.85	4.8	1.0719	11.54

3. Results and discussion

3.1. Phase stability and structure

Before assessment of vacancies, the stability and properties of the perfect solid solutions are investigated. The various properties will be subsequently used to assess the impact on vacancy formation enthalpies. The solid solution formability of high entropy alloys has been estimated via various parametric approaches in the past [52–54]. We calculate the solid solution mixing enthalpy, ΔH_{mix}, for equiatomic alloys via the regular solid solution model given by Yang et al. [54], ideal configurational entropy, ΔS_{conf}, valence electron concentration [53], (VEC), atomic size mismatch parameter, δ, solid solution formability parameter at the theoretical melting point [54], Ω, and the atomic packing parameter, γ [55].

$$\Delta H_{mix} = \sum_{i=1,\ i\neq j}^{n} 4\Delta H_{ij}^{mix} c_i c_j \tag{4}$$

$$\Delta S_{conf} = -R\sum_{i=1}^{n}(c_i \ln(C_i)) \tag{5}$$

$$VEC = \sum_{i=1}^{n} c_i (VEC)_i \tag{6}$$

$$\delta = 100 \times \sqrt{\sum_{i=1}^{n} c_i \left(1 - \frac{r_i}{\bar{r}}\right)^2} \tag{7}$$

$$\Omega = \frac{T_m \Delta S_{mix}}{|\Delta H_{mix}|};\ T_m = \sum_{i=1}^{n} c_i (T_m)_i \tag{8}$$

$$\omega_s = 1 - \sqrt{\frac{(r_L + \bar{r})^2 - \bar{r}^2}{(r_L + \bar{r})^2}};\ \omega_L = 1 - \sqrt{\frac{(r_s + \bar{r})^2 - \bar{r}^2}{(r_s + \bar{r})^2}};\ \gamma = \frac{\omega_s}{\omega_L} \tag{9}$$

Where c_i and c_j are the atomic fractions of elements i and j, respectively. ΔH_{ij}^{mix} is the enthalpy of mixing of binary liquid alloys, based on the Miedema macroscopic model for liquid binary alloys obtained from Takeuchi et al. [56]. R is the ideal gas constant in JK^{-1}mol^{-1}, $(VEC)_i$ is the valence electron concentration of the i^{th} element, $\bar{r} = \Sigma_{i=1}^{n} c_i r_i$ is the average atomic radius and r_i is the atomic radius of element i, $(T_m)_i$ is the melting point of the i^{th} element.

Table 2
Lattice constant of refractory alloys calculated via the volume averaging scheme.

composition	lattice constant (Å)
HfMoNbTaTi	3.31±0.01
HfMoNbTaW	3.29±0.01
HfMoNbTaZr	3.38±0.01
HfMoNbTiW	3.28±0.01
HfMoNbTiZr	3.36±0.01
HfMoNbWZr	3.34±0.01
HfMoTaTiW	3.28±0.01
HfMoTaTiZr	3.37±0.01
HfMoTaWZr	3.35±0.01
HfMoTiWZr	3.34±0.01
HfNbTaTiW	3.32±0.01
HfNbTaTiZr	3.41±0.01
HfNbTaWZr	3.38±0.01
HfNbTiWZr	3.38±0.01
HfTaTiWZr	3.37±0.01
MoNbTaTiW	3.23±0.01
MoNbTaTiZr	3.32±0.01
MoNbTaWZr	3.30±0.01
MoNbTiWZr	3.28±0.01
MoTaTiWZr	3.29±0.01
NbTaTiWZr	3.32±0.01

The putative boundaries for each parameter for solid-solution formation are: $-15\ kJmol^{-1} < \Delta H_{mix} < 5\ kJmol^{-1}$ [52]; $12\ JK^{-1}mol^{-1} < \Delta S_{mix} < 17.5\ JK^{-1}mol^{-1}$ [52,54]; VEC ≤ 6.87 for body-centred cubic structures, VEC ≥ 8 for face-centred cubic structures [53]; $\delta \leq 6.6\%$ [52]; $\Omega \geq 1.1$ [54]; and $\gamma \leq 1.175$ [55]. The calculated values for the thermophysical parameters in the present alloys are in Table 1.

All present alloys satisfy the boundaries for solid solution phase formation for ΔH_{mix}, ΔS_{conf}, Ω, and γ. VEC of the alloys are below 6.87 which suggests a body-centred cubic is preferred [53]. The alloys HfMoNbTiZr, HfMoTaTiZr, and HfMoTiWZr have δ values of 6.68, 6.73, and 6.7, respectively, which suggest these alloys may not form solid solutions. HfNbTaTiZr has a positive mixing enthalpy of $\Delta H_{mix} = +2.72\ kJmol^{-1}$ which suggests a miscibility gap at 0 K.

The parametric method suggests that the alloys investigated in this paper produce stable body-centred cubic solutions. However, there is a lack of information regarding the thermal stability of the alloys that were investigated in this work. It is possible for local ordering, precipitation, segregation, and clustering of elements to occur, which will influence the vacancy energetics within the alloy. HfNbTaTiZr, for instance, has a positive ΔH_{mix}, indicating a thermodynamic tendency to decompose at low temperatures. MoNbTaTiW is known to undergo B2-like ordering at intermediate temperatures, which may influence the vacancy formation enthalpies of this alloy. Vacancy sinks, such as grain boundaries, are another factor that has an impact on the vacancy concentrations in concentrated solid solutions. Additionally, vacancy migration contributes to the observed vacancy concentrations in real materials. Migration is affected by dislocation density [57], clustering of vacancies, and the presence of defect sinks like grain boundaries.

3.2. Calculating lattice constants

There is no generally agreed upon method in literature for calculating lattice constants for HEAs or alloys in general. Experimentally, this is normally determined via a technique such as X-ray diffraction where the maximum peak intensity points are used to assess the general structure of the material. Lattice constants for the alloys in this study were predicted via three methods:

1 The cube root of the total supercell volume is taken and divided by the unit cell width (3 for a $3 \times 3 \times 3$ cubic supercell) and this is taken as an estimate for the lattice constant across the cell.

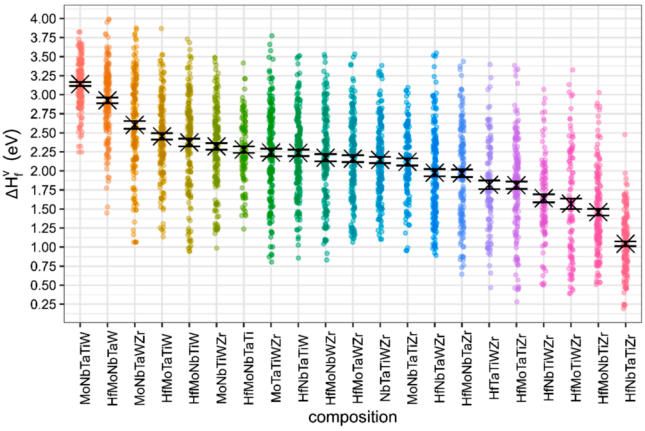

Fig. 2. Vacancy formation enthalpy for equiatomic alloys in the Hf-Mo-Nb-Ta-Ti-W-Zr system. H_f^v values are ordered from highest to lowest. A cross indicates mean H_f^v values for each alloy. Error bars indicate standard error of the mean.

2 All neighbour distances across the cell are measured and the mean of those expected around the 2nd nearest neighbour (similar treatment to Wang et al. [27]) are taken to be representative of the alloy.
3 The rule of mixtures (Vegard's law [58]) is applied to lattice constants of fully relaxed body-centred cubic supercells of pure elements in the Hf-Mo-Nb-Ta-Ti-W-Zr system. This third method is known to neglect the influence of lattice distortion on the crystal and is therefore likely to overpredict lattice parameter of concentrated solid solution alloys.

A discussion of methods to calculate the lattice constant in high entropy alloy supercells is found in **Supplementary Figure S4**. It was found that by cube rooting the volume and dividing by the unit cell width (Method 1), was able to provide an average lattice constant whilst taking into account the distortion of the lattice. The lattice constant of the present alloys is in Table 2. The volume averaging scheme was used for subsequent correlation studies.

3.3. Vacancy formation enthalpies

At least 2 unique special quasi-random cells were generated for each of the 21 alloys in the study. To determine if each special quasi-random cell produced enthalpies likely from the same population distribution, we performed a two-tailed Kolmogorov-Smirnov test between each sample distribution (**Supplementary Table S2**). After confirming we likely adequately sampled the same probability distribution for each alloy, we combined each sample distribution to produce a single distribution of energies for each alloy. For completeness, the vacancy formation enthalpies for the pure hexagonal close packed (Hf: 2.20; Ti: 2.04; and Zr: 1.98 eV) and body-centred cubic (Mo: 2.80; Nb: 2.62; Ta: 2.83; and W: 3.33 eV) elements were calculated.

The vacancy formation enthalpy adopts a single value in pure elements. However, the local chemical variations in concentrated solid solutions produce a distribution of vacancy formation enthalpies. The calculated enthalpies of the quinary Hf-Mo-Nb-Ta-Ti-W-Zr alloys are in Fig. 2 (ordered from highest to lowest mean values for H_f^v) The largest mean H_f^v belongs to MoNbTaTiW, which, incidentally, is the most reported quinary refractory alloy in literature [59–62]. The mean H_f^v for MoNbTaTiW is 3.14 eV and is similar to body-centred cubic W (3.11 [63] – 3.19 [64] via density functional theory, and 3.1 - 3.4 eV experimentally [65]). HfNbTaTiZr exhibited the lowest mean enthalpy of vacancy formation of 1.04 eV which is similar to low melting face-centred cubic elements like Cu (1.33 eV) and Ag (0.96 eV) [66]. This indicates the possible low thermal stability of these solid solutions, and the high probability that these alloys either have a low relative melting point

Table 3
Mean H_f^v values for concentrated solid solutions. Where σ is the standard deviation of the mean H_f^v.

composition	*mean* H_f^v *(eV)*	σ*(eV)*
MoNbTaTiW	3.14	0.32
HfMoNbTaW	2.93	0.48
MoNbTaWZr	2.60	0.65
HfMoTaTiW	2.45	0.54
HfMoNbTiW	2.37	0.64
MoNbTiWZr	2.32	0.56
HfMoNbTaTi	2.28	0.44
HfNbTaTiW	2.24	0.54
MoTaTiWZr	2.24	0.63
HfMoNbWZr	2.17	0.60
HfMoTaWZr	2.16	0.57
NbTaTiWZr	2.14	0.52
MoNbTaTiZr	2.12	0.50
HfNbTaWZr	1.98	0.60
HfMoNbTaZr	1.97	0.63
HfTaTiWZr	1.82	0.61
HfMoTaTiZr	1.81	0.62
HfNbTiWZr	1.64	0.55
HfMoTiWZr	1.57	0.72
HfMoNbTiZr	1.46	0.55
HfNbTaTiZr	1.04	0.39

compared to alloys in this study, or that they decompose into more stable, multiphase systems The rest of the solid solutions considered in this study exhibited intermediate H_f^v, with mean values from 1.46 – 2.93 eV. Mean values of H_f^v for all alloys in this study are in Table 3.

There is little correlation between H_f^v and the element being removed [27]. However, H_f^v does depend on the elements which make up the nearest neighbour environment. For example, Hf, Ti, and Zr have vacancy formation enthalpies of 2.20, 1.98, and 2.04 eV, respectively. When these elements form the nearest neighbour environment, H_f^v is likely to decrease. In contrast, the presence of Mo and W as neighbouring elements (with H_f^v values of 2.80 and 3.33 eV, respectively), is likely to increase H_f^v. Therefore, the resulting vacancy formation energy appears to be the result of an averaging scheme based on the local environment. **Supplementary Figure S5** shows the product-moment correlation coefficients of nearest neighbour elements versus the calculated H_f^v for each environment. Local element bias was found to have no direct correlation with H_f^v, as a strong bias toward a particular element shifts the enthalpy of vacancy formation towards that of the biased element.

Local properties surrounding each vacancy were collected (vacancy volume, immediate neighbour atoms) as well as bulk properties of the alloys (valence electron concentration, lattice constant, average electron shell number, atomic size mismatch factor, δ, amongst others). The thermophysical parameters are found in Table 1. Fig. 3 shows that the mean H_f^v of the studied alloys strongly correlates with valence electron concentration (Fig. 3a: $r = 0.88$), number of hexagonal close packed alloying elements (Fig. 3b: $r = -0.91$), and lattice constant (Fig. 3c: $r = -0.87$). Vacancy volume, calculated from the convex hull between atomic coordinates of atoms within 2.75 Å around the removed atom, was found to weakly correlate with H_f^v ($r = +0.28$; **Supplementary Figure S6).**

H_f^v is largely dependant on the first nearest neighbours [67]. This suggests that element clustering and segregation have a significant role in defining the vacancy energies of real materials. In addition, the enthalpies at the lower end of the distribution have a greater impact on the equilibrium vacancy concentration. Future research should make a concerted effort to sample these smaller enthalpies. The enthalpy of vacancy formation has been found to correspond with bulk parameters such as lattice constant, valence electron concentration, and several Hume-Rothery factors including the preferred crystal structure of the constituent elements at 0 K. These parameters may be used as a simple empirical relation to estimate H_f^v as a first approximation.

3.4. Population of vacancies in Hf-Mo-Nb-Ta-Ti-W-Zr quinary alloys

The value of H_f^v can be used to estimate probability of vacancy formation and therefore the vacancy concentration, X_i, in a material [68]. Similar to Daigle *et al.*, we calculate the vacancy concentration in equiatomic concentrated solid solutions with the configurational entropy of the added monovacancy (Eq. (10)) [20]. Furthermore, we compute the vacancy concentration using the entire enthalpy distribution, which takes into account the preferential formation of vacancies with enthalpies at the lower tail of the H_f^v distribution (Eq. (11)).

$$X_i = \frac{n}{N} = \frac{1}{m} e^{\frac{-\Delta H_f^v}{k_B T}} \tag{10}$$

$$X_i = \frac{n}{N} = \frac{\sum_{i=1}^{n} \frac{1}{m} e^{\frac{-\Delta H_f^v(i)}{k_B T}}}{n} \tag{11}$$

where $\frac{n}{N}$ is the fraction of vacancies in the system, m is the alloying

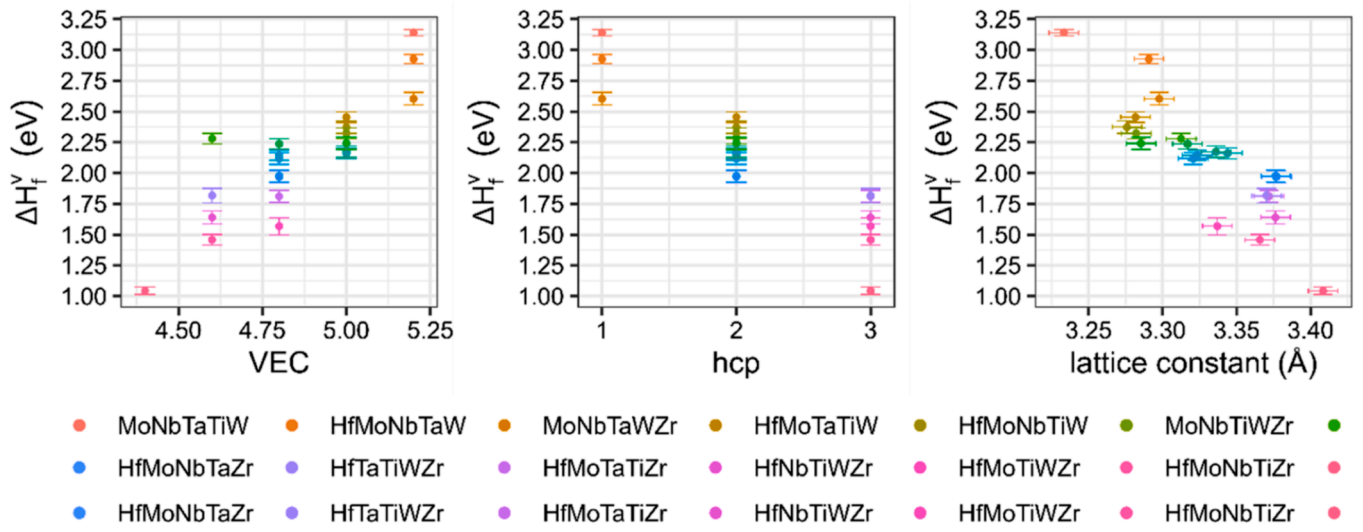

Fig. 3. Mean H_f^v values for alloys in the Hf-Mo-Nb-Ta-Ti-W-Zr system plotted versus a) valence electron concentration; b) number of constituent hexagonal close packed elements; and c) calculated lattice constant. Vertical error bars indicate the standard error of the mean of H_f^v; horizontal error bars indicate maximum deviation observed in lattice parameter across all the alloys.

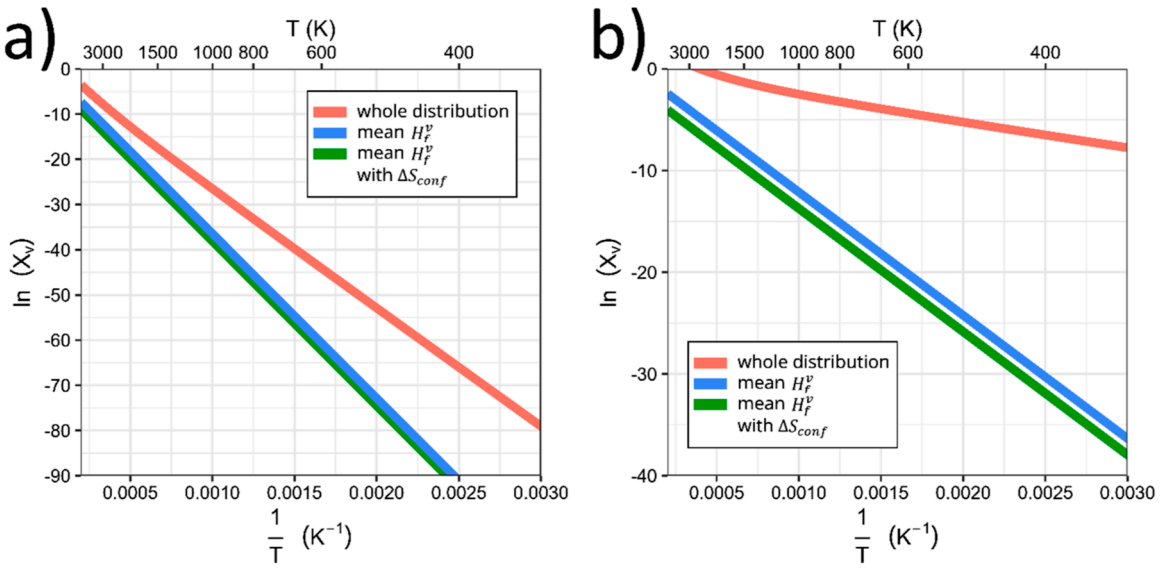

Fig. 4. Equilibrium vacancy concentration versus temperature. For a) MoNbTaTiW; and b) HfNbTaTiZr. X_v is the equilibrium vacancy concentration, $X_v = \frac{n}{N}$.

number, ΔH_f^v is the mean enthalpy of monovacancy formation (eV), k_B is the Boltzmann constant (eVK^{-1}), T is temperature (K), $\Delta H_f^v(i)$ is the enthalpy of vacancy formation for the i^{th} observation, and n is the number of observations. Eq. (10) considers the configurational entropy of adding a vacancy to an m number of elements at the dilute limit and is with accordance to the $m+1$ species scheme [69]. Adding a vacancy to concentrated solid solutions results in a lower additional configurational entropy with increasing m (**Supplementary Figure S7**). The derivation for Eq. (10) is given in **Supplementary Appendix 1**.

We calculate the equilibrium vacancy concentration here for two alloys, MoNbTaTiW, and HfNbTaTiZr, using a) the mean H_f^v only; b) with the additional configurational entropy of the vacancy; and c) by using the entire distribution of H_f^v. From Fig. 4a, the configurational entropy associated with monovacancies in complex materials reduces their concentration in the MoNbTaTiW alloy compared with pure metals and dilute alloys. However, when the entire distribution of energies is considered, there is a significantly higher concentration of vacancies throughout the entire temperature range. This is because vacancies with lower formation enthalpies preferentially form within the alloy crystal, and therefore contribute most to the equilibrium vacancy concentration. Likewise, the same effect can be seen in Fig. 4b for HfNbTaTiZr. In both cases, the equilibrium vacancy concentration significantly deviates from typical Arrhenius behaviour especially at temperatures > 2000 K. This non-Arrhenius dependence of vacancy concentration is found to be characteristic for all HEAs in the present study (**Supplementary Figure S8**) and may be a general property of all high entropy systems such as high entropy alloys and high entropy ceramics.

By considering the entire distribution of monovacancy formation in HEAs, it is possible to compute an effective H_f^v as if the solid solution were a pure element. For the alloys in this study, this result is significantly lower than the mean H_f^v that is typically used previously to predict vacancies in pure elements and dilute alloys:

$$H_f^v(\text{effective}) = -k_B T \ln\left(\frac{\sum_{i=1}^{n} \frac{1}{m} e^{\frac{-\Delta H_f^v(i)}{k_B T}}}{n}\right) \tag{12}$$

where $\Delta H_f^v(i)$ is the enthalpy of vacancy formation for the i^{th}

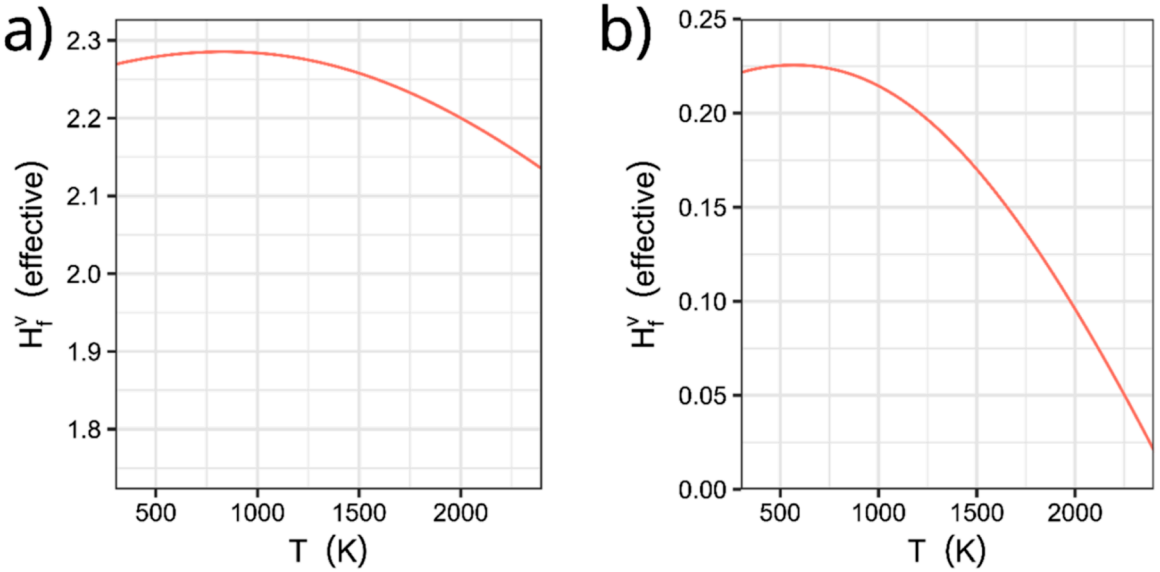

Fig. 5. Effective H_f^v versus temperature. For a) MoNbTaTiW; and b) HfNbTaTiZr.

observation, and n is the number of observations. We compute the effective H_f^v for MoNbTaTiW and HfNbTaTiZr using Eq. (12). Fig. 5a depicts the temperature dependence of the effective H_f^v for MoNbTaTiW. An effective H_f^v below 3.14 eV for MoNbTaTiW implies that monovacancies form much more easily at lower temperatures than if a simple average H_f^v is used. Similarly, Fig. 5b illustrates effective H_f^v for HfNbTaTiZr. In both cases, the effective H_f^v is significantly lower than the mean H_f^v (MoNbTaTiW: 3.14 eV; HfNbTaTiZr: 1.04 eV).

Our findings indicate that the higher equilibrium concentration of monovacancies observed experimentally in HEAs is primarily driven by the spread of vacancy formation enthalpies (H_f^v) inherent in these materials. Specifically, the deviation of the effective H_f^v from the mean H_f^v increases with the spread of H_f^v values (for example, shown in Fig. 2), resulting in more vacancies than those predicted for simple pure metals and conventional alloys.

Summary

In this work, we examine the vacancy formation enthalpies and associated equilibrium vacancy concentrations of quinary alloys in the Hf-Mo-Nb-Ta-Ti-W-Zr system using density functional theory calculations. It is shown that while configurational entropy reduces vacancy concentration in these multicomponent systems, the lower tails in the enthalpy distribution caused by complex local environments around each vacancy lead to superabundant vacancies. This mechanism is likely to be active in both ordinary alloys and compositionally complex materials. This work provides insight into vacancy formation and equilibrium vacancy concentrations of high entropy alloys. Future analyses will investigate local ordering of elements and its effect on vacancy concentration.

Declaration of Competing Interest

The authors declare that they have no known competing financial interests or personal relationships that could have appeared to influence the work reported in this paper.

Acknowledgments

JAW is funded through the Nuclear Energy Futures Centre for Doctoral Training (EP/S023844/1), co-sponsored by the National Nuclear Laboratory (NNL). SCM is funded through the Sêr Cymru II programme by Welsh European Funding Office (WEFO) under the European Regional Development Fund (ERDF). CM is funded through the Knowledge Economy Skills Scholarships (KESS 2) programme which is part funded through the Welsh government's European Social Fund (ESF). Computing resources were made available by Supercomputing Wales operated by Cardiff University (www.supercomputing.wales) and by the Cambridge Service for Data Driven Discovery (CSD3) operated by the University of Cambridge Research Computing Service (www.csd3.cam.ac.uk).

Supplementary materials

Supplementary material associated with this article can be found, in the online version, at doi:10.1016/j.mtla.2023.101764.

References

[1] B. Cantor, I.T.H. Chang, P. Knight, A.J.B. Vincent, Microstructural development in equiatomic multicomponent alloys, Mater. Sci. Eng. A. 375–377 (2004) 213–218, https://doi.org/10.1016/j.msea.2003.10.257.

[2] J.W. Yeh, S.K. Chen, S.J. Lin, J.Y. Gan, T.S. Chin, T.T. Shun, C.H. Tsau, S.Y. Chang, Nanostructured high-entropy alloys with multiple principal elements: novel alloy design concepts and outcomes, Adv. Eng. Mater. 6 (2004) 299–303, https://doi.org/10.1002/adem.200300567. +274.

[3] J. Wilson, L. Evitts, M. Rushton, D. Goddard, S. Middleburgh, W. Lee, High entropy alloys for accident tolerant fuel applications, in: TopFuel, TopFuel 2021, 2021. https://www.researchgate.net/publication/361225055_High_entropy_alloys_for_accident_tolerant_fuel_applications (accessed July 19, 2022).

[4] E.J. Pickering, A.W. Carruthers, P.J. Barron, S.C. Middleburgh, D.E.J. Armstrong, A.S. Gandy, High-entropy alloys for advanced nuclear applications, Entropy 23 (2021) 1–28, https://doi.org/10.3390/e23010098.

[5] M. Dada, P. Popoola, S. Adeosun, N. Mathe, M. Dada, P. Popoola, S. Adeosun, N. Mathe, High entropy alloys for aerospace applications, IntechOpen, n.d. www.intechopen.com (accessed June 7, 2021).

[6] M.H. Tsai, J.W. Yeh, High-entropy alloys: a critical review, Mater. Res. Lett. 2 (2014) 107–123, https://doi.org/10.1080/21663831.2014.912690.

[7] Y.J. Zhou, Y. Zhang, Y.L. Wang, G.L. Chen, Solid solution alloys of AlCoCrFeNi Tix with excellent room-temperature mechanical properties, Appl. Phys. Lett. 90 (2007), 181904, https://doi.org/10.1063/1.2734517.

[8] F. Müller, B. Gorr, H.-J.J. Christ, J. Müller, B. Butz, H. Chen, A. Kauffmann, M. Heilmaier, On the oxidation mechanism of refractory high entropy alloys, Corros. Sci. 159 (2019), 108161, https://doi.org/10.1016/j.corsci.2019.108161.

[9] F. Müller, B. Gorr, H.J. Christ, H. Chen, A. Kauffmann, M. Heilmaier, Effect of Y additions on the oxidation behaviour of novel refractory high-entropy alloy NbMoCrTiAl at 1000°C in air, Oxid. Met 94 (2020) 147–163, https://doi.org/10.1007/S11085-020-09983-6/FIGURES/10.

[10] T.M. Butler, M.L. Weaver, Oxidation behavior of arc melted AlCoCrFeNi multi-component high-entropy alloys, J. Alloys Compd. 674 (2016) 229–244, https://doi.org/10.1016/j.jallcom.2016.02.257.

[11] T.M. Butler, K.J. Chaput, J.R. Dietrich, O.N. Senkov, High temperature oxidation behaviors of equimolar NbTiZrV and NbTiZrCr refractory complex concentrated alloys (RCCAs), J. Alloys Compd. 729 (2017) 1004–1019, https://doi.org/10.1016/J.JALLCOM.2017.09.164.

[12] Z.D. Han, H.W. Luan, X. Liu, N. Chen, X.Y. Li, Y. Shao, K.F. Yao, Microstructures and mechanical properties of TixNbMoTaW refractory high-entropy alloys, Mater. Sci. Eng. A. 712 (2018) 380–385, https://doi.org/10.1016/j.msea.2017.12.004.

[13] B. Christiaen, C. Domain, L. Thuinet, A. Ambard, A. Legris, Influence of vacancy diffusional anisotropy: understanding the growth of zirconium alloys under irradiation and their microstructure evolution, Acta Mater. 195 (2020) 631–644, https://doi.org/10.1016/J.ACTAMAT.2020.06.004.

[14] W. Sun, Y. Zhu, R. Marceau, L. Wang, Q. Zhang, X. Gao, C. Hutchinson, Precipitation strengthening of aluminum alloys by room-temperature cyclic plasticity, Science 363 (80) (2019) 972–975, https://doi.org/10.1126/SCIENCE.AAV7086/SUPPL_FILE/AAV7086_SUN_SM.PDF.

[15] M.H. Cui, T.L. Shen, H.P. Zhu, J. Wang, X.Z. Cao, P. Zhang, L.L. Pang, C.F. Yao, K. F. Wei, Y.B. Zhu, B.S. Li, J.R. Sun, N. Gao, X. Gao, H.P. Zhang, Y.B. Sheng, H. L. Chang, W.H. He, Z.G. Wang, Vacancy like defects and hardening of tungsten under irradiation with He ions at 800°C, Fus. Eng. Des. 121 (2017) 313–318, https://doi.org/10.1016/J.FUSENGDES.2017.05.043.

[16] Q. Xu, H.Q. Guan, Z.H. Zhong, S.S. Huang, J.J. Zhao, Irradiation resistance mechanism of the CoCrFeMnNi equiatomic high-entropy alloy, Sci. Reports 111 (11) (2021) 1–8, https://doi.org/10.1038/s41598-020-79775-0, 2021.

[17] F. Ruicheng, C. Hui, L. Haiyan, R. Zhiyuan, Y. Changfeng, Effects of vacancy concentration and temperature on mechanical properties of single-crystal γ-TiAl based on molecular dynamics simulation, High Temp. Mater. Process. 37 (2018) 113–120, https://doi.org/10.1515/HTMP-2016-0156/MACHINEREADABLECITATION/RIS.

[18] J. Peng, B. Xie, X. Zeng, Q. Fang, B. Liu, P.K. Liaw, J. Li, Vacancy dependent mechanical behaviors of high-entropy alloy, Int. J. Mech. Sci. 218 (2022), 107065, https://doi.org/10.1016/J.IJMECSCI.2022.107065.

[19] Z. Wang, C.T. Liu, P. Dou, Thermodynamics of vacancies and clusters in high-entropy alloys, Phys. Rev. Mater. 1 (2017), 043601. https://journals.aps.org/prmaterials/abstract/10.1103/PhysRevMaterials.1.043601 (accessed September 11, 2021).

[20] S.E. Daigle, D.W. Brenner, Statistical approach to obtaining vacancy formation energies in high-entropy crystals from first principles calculations: application to a high-entropy diboride, Phys. Rev. Mater. 4 (2020), 123602, https://doi.org/10.1103/PHYSREVMATERIALS.4.123602/FIGURES/6/MEDIUM.

[21] D.E. Jodi, T.A. Listyawan, P. Hruska, J. Cizek, N. Park, U. Lee, Study of vacancies in Fex(CoCrMnNi)100-x medium- and high-entropy alloys by positron annihilation spectroscopy, Scr. Mater. 194 (2021), 113654, https://doi.org/10.1016/J.SCRIPTAMAT.2020.113654.

[22] K. Sugita, N. Matsuoka, M. Mizuno, H. Araki, Vacancy formation enthalpy in CoCrFeMnNi high-entropy alloy, Scr. Mater. 176 (2020) 32–35, https://doi.org/10.1016/J.SCRIPTAMAT.2019.09.033.

[23] M. Vaidya, K.G. Pradeep, B.S. Murty, G. Wilde, S.V. Divinski, Bulk tracer diffusion in CoCrFeNi and CoCrFeMnNi high entropy alloys, Acta Mater 146 (2018) 211–224, https://doi.org/10.1016/J.ACTAMAT.2017.12.052.

[24] X. Zhang, S.V. Divinski, B. Grabowski, Ab initio prediction of vacancy energetics in HCP Al-Hf-Sc-Ti-Zr high entropy alloys and the subsystems, Acta Mater. (2022), 117677, https://doi.org/10.1016/J.ACTAMAT.2022.117677.

[25] M. Mizuno, K. Sugita, H. Araki, Defect energetics for diffusion in CrMnFeCoNi high-entropy alloy from first-principles calculations, Comput. Mater. Sci. 170 (2019), 109163, https://doi.org/10.1016/J.COMMATSCI.2019.109163.

[26] D. Vizoso, C. Deo, Determination of vacancy formation energies in binary UZr alloys using special quasirandom structure methods, Front. Mater. 8 (2021) 243, https://doi.org/10.3389/FMATS.2021.692660/BIBTEX.

[27] Y. Wang, X. Li, X. Li, Y. Zhang, Y. Zhang, Y. Xu, Y. Lei, C.S. Liu, X. Wu, Prediction of vacancy formation energies at tungsten grain boundaries from local structure via

machine learning method, J. Nucl. Mater. 559 (2022), 153412, https://doi.org/10.1016/J.JNUCMAT.2021.153412.
[28] Y.Z. Wang, Y.J. Wang, Disentangling diffusion heterogeneity in high-entropy alloys, Acta Mater. 224 (2022), 117527, https://doi.org/10.1016/J.ACTAMAT.2021.117527.
[29] Y. Zhang, A. Manzoor, C. Jiang, D. Aidhy, D. Schwen, A statistical approach for atomistic calculations of vacancy formation energy and chemical potentials in concentrated solid-solution alloys, Comput. Mater. Sci. 190 (2021), 110308, https://doi.org/10.1016/J.COMMATSCI.2021.110308.
[30] W. Chen, X. Ding, Y. Feng, X. Liu, K. Liu, Z.P. Lu, D. Li, Y. Li, C.T. Liu, X.Q. Chen, Vacancy formation enthalpies of high-entropy FeCoCrNi alloy via first-principles calculations and possible implications to its superior radiation tolerance, J. Mater. Sci. Technol. 34 (2018) 355–364, https://doi.org/10.1016/J.JMST.2017.11.005.
[31] S.C. Middleburgh, D.M. King, G.R. Lumpkin, M. Cortie, L. Edwards, Segregation and migration of species in the CrCoFeNi high entropy alloy, J. Alloys Compd. 599 (2014) 179–182.
[32] A. Esfandiarpour, M.N. Nasrabadi, Vacancy formation energy in CuNiCo equimolar alloy and CuNiCoFe high entropy alloy: ab initio based study, Calphad. 66 (2019) 101634. https://doi.org/10.1016/J.CALPHAD.2019.101634.
[33] C. Li, J. Yin, K. Odbadrakh, B.C. Sales, S.J. Zinkle, G.M. Stocks, B.D. Wirth, First principle study of magnetism and vacancy energetics in a near equimolar NiFeMnCr high entropy alloy, J. Appl. Phys. 125 (2019), 155103, https://doi.org/10.1063/1.5086172.
[34] Z.-S. Nong, Z.-H. Gu, Y.-W. Liu, Z.-Y. Wang, J.-C. Zhu, Formation and migration behavior of vacancy in multi-component alloys, Intermetallics 151 (2022), 107724, https://doi.org/10.1016/J.INTERMET.2022.107724.
[35] A. Roy, P. Singh, G. Balasubramanian, D.D. Johnson, Vacancy formation energies and migration barriers in multi-principal element alloys, Acta Mater. 226 (2022), 117611, https://doi.org/10.1016/J.ACTAMAT.2021.117611.
[36] P. Singh, S. Gupta, S. Thimmaiah, B. Thoeny, P.K. Ray, A.V. Smirnov, D. D. Johnson, M.J. Kramer, Vacancy-mediated complex phase selection in high entropy alloys, Acta Mater. 194 (2020) 540–546, https://doi.org/10.1016/J.ACTAMAT.2020.04.063.
[37] A. Cunliffe, J. Plummer, I. Figueroa, I. Todd, Glass formation in a high entropy alloy system by design, Intermetallics 23 (2012) 204–207, https://doi.org/10.1016/J.INTERMET.2011.12.006.
[38] A.X. Lin-Vines, J.A. Wilson, A. Fraile, L.J. Evitts, M.J.D. Rushton, J.O. Astbury, W. E. Lee, S.C. Middleburgh, Defect behaviour in the MoNbTaVW high entropy alloy (HEA), Res. Mater. 15 (2022), 100320, https://doi.org/10.1016/J.RINMA.2022.100320.
[39] S. Zhao, Defect properties in a VTaCrW equiatomic high entropy alloy (HEA) with the body centered cubic (bcc) structure, J. Mater. Sci. Technol. 44 (2020) 133–139, https://doi.org/10.1016/j.jmst.2019.10.025.
[40] P. Hohenberg, W. Kohn, Inhomogeneous electron gas, Phys. Rev. 136 (1964) B864, https://doi.org/10.1103/PhysRev.136.B864.
[41] W. Kohn, L.J. Sham, Self-consistent equations including exchange and correlation effects, Phys. Rev. 140 (1965) A1133, https://doi.org/10.1103/PhysRev.140.A1133.
[42] A. Van De Walle, P. Tiwary, M. De Jong, D.L. Olmsted, M. Asta, A. Dick, D. Shin, Y. Wang, L.Q. Chen, Z.K. Liu, Efficient stochastic generation of special quasirandom structures, Calphad Comput. Coupling Phase Diagrams Thermochem. 42 (2013) 13–18, https://doi.org/10.1016/j.calphad.2013.06.006.
[43] G. Kresse, Ab initio molecular dynamics for liquid metals, J. Non. Cryst. Solids. 192–193 (1995) 222–229, https://doi.org/10.1016/0022-3093(95)00355-X.
[44] G. Kresse, J. Furthmüller, Efficiency of ab-initio total energy calculations for metals and semiconductors using a plane-wave basis set, Comput. Mater. Sci. 6 (1996) 15–50, https://doi.org/10.1016/0927-0256(96)00008-0.
[45] P.E. Blöchl, Projector augmented-wave method, Phys. Rev. B. 50 (1994) 17953–17979, https://doi.org/10.1103/PhysRevB.50.17953.
[46] G. Kresse, D. Joubert, From ultrasoft pseudopotentials to the projector augmented-wave method, Phys. Rev. B. 59 (1999) 1758, https://doi.org/10.1103/PhysRevB.59.1758.
[47] J.P. Perdew, K. Burke, M. Ernzerhof, Generalized gradient approximation made simple, Phys. Rev. Lett. 77 (1996) 3865–3868, https://doi.org/10.1103/PhysRevLett.77.3865.
[48] M. Methfessel, A.T. Paxton, High-precision sampling for Brillouin-zone integration in metals, Phys. Rev. B. 40 (1989) 3616–3621, https://doi.org/10.1103/PhysRevB.40.3616.
[49] D.J.M.M. King, S.C. Middleburgh, A.G. McGregor, M.B. Cortie, Predicting the formation and stability of single phase high-entropy alloys, Acta Mater. 104 (2016) 172–179, https://doi.org/10.1016/j.actamat.2015.11.040.
[50] N.P.Gurao Tazuddin, K. Biswas, In the quest of single phase multi-component multiprincipal high entropy alloys, J. Alloys Compd. 697 (2017) 434–442, https://doi.org/10.1016/J.JALLCOM.2016.11.383.
[51] R. Li, L. Xie, W.Y. Wang, P.K. Liaw, Y. Zhang, High-throughput calculations for high-entropy alloys: a brief review, Front. Mater. 7 (2020) 290, https://doi.org/10.3389/FMATS.2020.00290/BIBTEX.
[52] Y. Zhang, Y.J. Zhou, J.P. Lin, G.L. Chen, P.K. Liaw, Solid-solution phase formation rules for multi-component alloys, Adv. Eng. Mater. 10 (2008) 534–538, https://doi.org/10.1002/adem.200700240.
[53] S. Guo, C. Ng, J. Lu, C.T. Liu, Effect of valence electron concentration on stability of fcc or bcc phase in high entropy alloys, J. Appl. Phys. 109 (2011), https://doi.org/10.1063/1.3587228.
[54] X. Yang, Y. Zhang, Prediction of high-entropy stabilized solid-solution in multi-component alloys, Mater. Chem. Phys. 132 (2012) 233–238. https://linkinghub.elsevier.com/retrieve/pii/S0254058411009357 (accessed February 13, 2021).
[55] Z. Wang, Y. Huang, Y. Yang, J. Wang, C.T. Liu, Atomic-size effect and solid solubility of multicomponent alloys, Scr. Mater. 94 (2015) 28–31, https://doi.org/10.1016/j.scriptamat.2014.09.010.
[56] A. Takeuchi, A. Inoue, Classification of bulk metallic glasses by atomic size difference, heat of mixing and period of constituent elements and its application to characterization of the main alloying element, Mater. Trans. 46 (2005) 2817–2829. https://www.jstage.jst.go.jp/article/matertrans/46/12/46_12_2817/_article (accessed April 1, 2021).
[57] M. Glienke, M. Vaidya, K. Gururaj, L. Daum, B. Tas, L. Rogal, K.G. Pradeep, S. V. Divinski, G. Wilde, Grain boundary diffusion in CoCrFeMnNi high entropy alloy: kinetic hints towards a phase decomposition, Acta Mater. 195 (2020) 304–316, https://doi.org/10.1016/J.ACTAMAT.2020.05.009.
[58] A.R. Denton, N.W. Ashcroft, Vegard's law, Phys. Rev. A. 43 (1991) 3161, https://doi.org/10.1103/PhysRevA.43.3161.
[59] Z.D. Han, N. Chen, S.F. Zhao, L.W. Fan, G.N. Yang, Y. Shao, K.F. Yao, Effect of Ti additions on mechanical properties of NbMoTaW and VNbMoTaW refractory high entropy alloys, Intermetallics 84 (2017) 153–157, https://doi.org/10.1016/j.intermet.2017.01.007.
[60] I. Toda-Caraballo, A general formulation for solid solution hardening effect in multicomponent alloys, Scr. Mater. 127 (2017) 113–117, https://doi.org/10.1016/j.scriptamat.2016.09.009.
[61] A. Mishra, G. Priyadarshan, D. Clark, Y. Lu, R. Shi, Theoretical investigations on structural stability and elastic properties of MoNbTaW-X (=Ti/V) high entropy alloys, 2019. http://www.sdiarticle4.com/review-history/52208 (accessed October 11, 2020).
[62] U. Bhandari, C. Zhang, S. Guo, S. Yang, First-principles study on the mechanical and thermodynamic properties of MoNbTaTiW, Int. J. Miner. Metall. Mater. 27 (2020) 1398–1404, https://doi.org/10.1007/s12613-020-2077-1.
[63] C.S. Becquart, C. Domain, Ab initio calculations about intrinsic point defects and He in W, Nucl. Instrum. Methods Phys. Res. Sect. B Beam Interact. with Mater. Atoms. 255 (2007) 23–26, https://doi.org/10.1016/j.nimb.2006.11.006.
[64] W.H. He, X. Gao, N. Gao, J. Wang, D. Wang, M.H. Cui, L.L. Pang, Z.G. Wang, Effects of grain boundary characteristics on its capability to trap point defects in tungsten, Chin. Phys. Lett. 35 (2018), 026101, https://doi.org/10.1088/0256-307X/35/2/026101.
[65] K. Maier, M. Peo, B. Saile, H.E. Schaefer, A. Seeger, High–temperature positron annihilation and vacancy formation in refractory metals, 40 (2006) 701–728. https://doi.org/10.1080/01418617908234869.
[66] P.A. Korzhavyi, I.A. Abrikosov, B. Johansson, A. Ruban, H.L. Skriver, First-principles calculations of the vacancy formation energy in transition and noble metals, Phys. Rev. B. 59 (1999) 11693–11703, https://doi.org/10.1103/PhysRevB.59.11693.
[67] A. Manzoor, Y. Zhang, D.S. Aidhy, Factors affecting the vacancy formation energy in Fe70Ni10Cr20 random concentrated alloy, Comput. Mater. Sci. 198 (2021), 110669, https://doi.org/10.1016/J.COMMATSCI.2021.110669.
[68] M.A. Tschopp, K.N. Solanki, F. Gao, X. Sun, M.A. Khaleel, M.F. Horstemeyer, Probing grain boundary sink strength at the nanoscale: energetics and length scales of vacancy and interstitial absorption by grain boundaries in α-Fe, Phys. Rev. B - Condens. Matter Mater. Phys. 85 (2012), 064108, https://doi.org/10.1103/PHYSREVB.85.064108/FIGURES/15/MEDIUM.
[69] C.M. Rost, E. Sachet, T. Borman, A. Moballegh, E.C. Dickey, D. Hou, J.L. Jones, S. Curtarolo, J.P. Maria, Entropy-stabilized oxides, Nat. Commun. 61 (6) (2015) 1–8, https://doi.org/10.1038/ncomms9485, 2015.